JOURNAL OF AIRCRAFT
Vol. 38, No. 4, July–August 2001

Numerical Simulation of Aircraft Trailing Vortices Interacting with Ambient Shear or Ground

M. Mokry*
National Research Council, Ottawa, Ontario K1A 0R6, Canada

A two-dimensional algorithm, based on the continuous vortex sheet method, is proposed for modeling the evolution and propagation of aircraft trailing vortices in a sheared environment. Among the phenomena discussed are the generation of secondary vortices, shear-layer instabilities, and interactions of trailing vortices with atmospheric and ground shear layers. Numerical simulations are produced by a code written as an interactive-graphics application for the Windows platform.

Nomenclature

A_n = loading coefficient
AR = wing aspect ratio
a_n = normalized loading coefficients
b = wing span
C = oriented vortex sheet
$\mathcal{C}$ = Courant number, Eq. (31)
C_L = lift coefficient
d = downstream distance, Eq. (30)
f = Cauchy density, Eq. (2)
i = $\sqrt{(-1)}$
t = real time, Eq. (29)
U = aircraft velocity
v_n = normal velocity
v_t = tangential velocity
w = complex velocity
x = spanwise (horizontal) coordinate
y = vertical coordinate
z = $x + iy$, complex coordinate
α = step function, Eq. (19)
Γ = spanwise circulation, Eq. (24)
γ = nondimensional vortex density, Eq. (27)
ζ = complex coordinate (contour point)
θ = polar angle, Eq. (25)
ν = angle between a normal to C and real axis
τ = pseudotime
Ω = analytic function

Subscripts

g = ground
s = shear
∞ = far

Superscripts

k = time-step index
$+$ = value to the left of C (above)
$-$ = value to the right of C (below)
$*$ = complex conjugate

Presented as Paper 99-0827 at the AIAA 37th Aerospace Sciences Meeting and Exhibit, Reno, NV, 11–14 January 1999; received 2 March 2000; revision received 10 January 2001; accepted for publication 20 January 2001.

*Group Leader, Experimental Aerodynamics and Aeroelasticity, Institute for Aerospace Research. Associate Fellow AIAA.

I. Introduction

THE two-dimensional vortex sheet method,[1] based on a line distribution of vorticity, is one of the simplest numerical methods that can be used to simulate the aircraft trailing vortices and their interactions with ambient shear with any degree of realism. It models the evolution of vortices in the crossflow (Trefftz) plane, in the infinite Reynolds number limit. In this limit the shear layer is contracted into a two-dimensional line distribution of vorticity, convected in an otherwise irrotational fluid.

The main advantages of the continuous sheet method over the discrete vortex method[2,3] is that the logarithmic singularity created at the corners of the segmented vortex sheet is weaker than that of isolated point vortices and that the jump of tangential velocity across the sheet is properly modeled.

As observed by Prandtl and Tietjens,[4] "the connection between vortex motion and the surfaces of discontinuity of potential motion lies in the fact that any small internal friction changes the discontinuity in velocity into a gradual transition in a layer with rotation. In the domain in which this continuous change takes place we have a layer of vorticity formed out of vortex filaments, whereas outside the layer there is potential flow." A more recent analysis of the connection between thin vortex layers and vortex sheets has been given by Baker and Shelley.[5]

Mathematically, a line of tangential discontinuity is known to be unstable[6–9] to small periodic disturbances (Kelvin–Helmholtz instability) and tends to disintegrate into a row of vortices. However, contrary to the discrete vortex method, the descendant vortices are not arbitrarily located point singularities, but rather finite-size structures that effectively increase the thickness of the original vortex sheet. Because stretching (elongation) has a stabilizing effect,[10–12] it is possible to simulate numerically a fairly regular evolution of vortex spirals by selecting sufficiently small time steps. Large time steps are found to lead to a chaotic labyrinth pattern in the core of the vortex during the initial roll up.

The discontinuity of the tangential velocity across the sheet plays a key role in rendering the internal structure of the vortex. When approaching the vortex center in the radial direction, the successive crossings of the spiral turns are accompanied by a decrease in tangential velocity, like in real, rotational flows.

The continuous sheet method described in this paper is not capable of capturing all complexities of vortex flows, such as effects of stratification or viscosity. In the present form the computational scheme conserves vorticity, that is vorticity is neither created at the boundaries nor diffused in the flowfield. However, it does satisfy two of the important principles recently outlined by Sarpkaya,[13] namely that the vortex core is constructed as an active fluid volume and the deformation of large flow structures is permitted. In an earlier study[14] it has been demonstrated that the mechanism for generating the secondary roll up is in fact a local contraction of the vortex sheet accompanied by a rapid peaking of the vortex density

function. The susceptibility of the contraction portions of the sheet to disintegration into smaller secondary vortices can also play an important role in the spiral-type breakdown of the vortex.

Based on extensive computational fluid dynamics (CFD) studies, Darracq et al.[15] suggested that the effect of viscosity on vortex trajectories and the interactions with shear layers at high Reynolds numbers is relatively minor, thus providing a numerical justification for the approximations based on an inviscid motion of thin vortex sheets. Near the ground, where the viscosity plays an important role, the inviscid-flow approach is applicable only when the ground shear layer, representing the boundary-layer displacement effect in crosswind, is known a priori.

II. Continuous Sheet Method

In the crossflow (Trefftz) plane the complex velocity induced by the vortex sheet C is represented by the line distribution of vorticity

$$w(z) = \int_C \frac{i\gamma(\zeta)}{2\pi(\zeta - z)} |d\zeta| \tag{1a}$$

where $|d\zeta|$ is the arc length element of C. The real-valued vortex density γ is positive if the vortex sheet element turns flow counterclockwise and negative if it turns flow clockwise. The complex contour element can be expressed as

$$d\zeta = |d\zeta|[-\sin\nu(\zeta) + i\cos\nu(\zeta)] = |d\zeta|\, ie^{i\nu(\zeta)}$$

where ν is pointing to the right, as indicated in Fig. 1. If z is a point of the vortex sheet C, the complex velocity is calculated by taking the principal value of the integral. This is consistent with the kinematics of vortex sheets, in which a vortex particle influences its own motion only through the displacements of other particles (mutual induction).

Most theoretical analyses interpret Eq. (1a) as the Birkhoff–Rott integro-differential equation,[9] where $\gamma|d\zeta| = d\gamma$, and the complex coordinates of the vortex sheet points are parametrized as $\zeta = \zeta(\gamma, t)$ and $z = z(\gamma, t)$. In the numerical approach of this paper, Eq. (1a) is used in its original form, together with the alternative representation

$$w(z) = \frac{1}{2\pi i} \int_C \frac{f(\zeta)}{\zeta - z}\, d\zeta \tag{1b}$$

where

$$f(\zeta) = i\gamma(\zeta)\, e^{-i\nu(\zeta)} \tag{2}$$

is the complex density function defined on C. The integral of Eq. (1b), recognized as that of Cauchy type, describes the function w, which is analytic everywhere except across C. In accordance with the Plemelj formula,[16]

$$w^+(\zeta) - w^-(\zeta) = f(\zeta) \tag{3}$$

where the superscripts + and − designate the limiting values of w to the left and right of C, respectively. Along C, as may be verified from appropriate velocity triangles,

$$w(\zeta) = [v_n(\zeta) - iv_t(\zeta)]\, e^{-i\nu(\zeta)} \tag{4}$$

Using Eqs. (2–4), it follows for the differences of normal and tangential velocities across the sheet

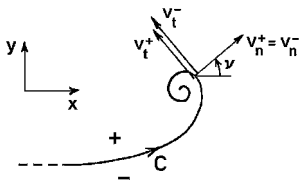

Fig. 1 Schematic of a vortex spiral.

$$v_n^+(\zeta) - v_n^-(\zeta) = 0, \qquad v_t^+(\zeta) - v_t^-(\zeta) = -\gamma(\zeta) \tag{5}$$

The numerical algorithm discretizes the vortex sheet by straight-line segments, replacing Eq. (1b) by the sum

$$w(z) = \sum_j w_j(z) \tag{6}$$

where

$$w_j(z) = \frac{1}{2\pi i} \int_{\zeta_{j-1}}^{\zeta_j} \frac{f(\zeta)}{\zeta - z}\, d\zeta \tag{7}$$

is the complex velocity induced by the jth segment. Assuming $f(\zeta) = f_j = \text{constant}$ on the segment,

$$w_j(z) = \frac{f_j}{2\pi i} \int_{\zeta_{j-1}}^{\zeta_j} \frac{d\zeta}{\zeta - z} = \frac{f_j}{2\pi i} \ln \frac{\zeta_j - z}{\zeta_{j-1} - z} \tag{8}$$

From Eq. (2)

$$f_j = ie^{-i\nu_j}\, \gamma_j \tag{9}$$

where

$$ie^{-i\nu_j} = i(\cos\nu_j - i\sin\nu_j) = -\frac{\zeta_j^* - \zeta_{j-1}^*}{|\zeta_j - \zeta_{j-1}|}$$

Accordingly,

$$w_j(z) = \frac{i\gamma_j}{2\pi} \frac{\zeta_j^* - \zeta_{j-1}^*}{|\zeta_j - \zeta_{j-1}|} \ln \frac{\zeta_j - z}{\zeta_{j-1} - z} \tag{10}$$

If z is an interior point of the segment ζ_{j-1}, ζ_j, the corresponding principal value is obtained by formally changing the logarithmic term in Eq. (8) as[17]

$$\ln \frac{\zeta_j - z}{\zeta_{j-1} - z} \rightarrow \ln \frac{\zeta_j - z}{z - \zeta_{j-1}}$$

If z is the segment midpoint, the principal value of Eq. (10) is then

$$w_j\left[\tfrac{1}{2}(\zeta_j + \zeta_{j-1})\right] = 0 \tag{11}$$

However, $w(z)$ remains singular not only at the vortex sheet endpoints, but also at the corner points of the segmented vortex sheet. From Eq. (8) the complex velocity induced by the two segments adjacent to ζ_j is

$$w_j(z) + w_{j+1}(z) = \frac{f_j}{2\pi i} \ln \frac{\zeta_j - z}{\zeta_{j-1} - z} + \frac{f_{j+1}}{2\pi i} \ln \frac{\zeta_{j+1} - z}{\zeta_j - z}$$

The logarithmic singularity at ζ_j is removable if

$$f_j = f_{j+1}$$

Assuming $|\nu_{j+1} - \nu_j| < \pi$, this, according to Eq. (9), can only be the case if

$$\gamma_j = \gamma_{j+1}, \qquad \nu_j = \nu_{j+1}$$

In other words, ζ_j would have to be an interior point of the straight-line segment ζ_{j-1}, ζ_{j+1}, which is in general impossible. Nevertheless, the logarithmic singularity of the "true" corner point is always weaker than that of a simple pole, as can be verified from the limit

$$\lim_{z \to \zeta} \frac{\ln|\zeta - z|}{|\zeta - z|^{-1}} = 0$$

Accordingly, the corner points of a segmented vortex sheet do not perturb the flow locally as much as isolated point vortices. A continuous, piecewise linear distribution of γ was considered but found of little benefit as the corresponding f is still dicontinuous at the corner points of segments, which have different slopes. However, further improvement might be possible by "desingularizing" the vortex sheet by introducing diffusion.[18]

The effect of crosswind or boundaries can be represented by an analytic function $\Omega(z)$ appended to Eq. (1a):

$$w(z) = \int_C \frac{i\gamma(\zeta)}{2\pi(\zeta - z)}|d\zeta| + \Omega(z) \tag{12}$$

For uniform crosswind

$$\Omega(z) = \text{real constant} \tag{13}$$

For the ground located at $y = y_g$, using the "underground" image of the vortex sheet,

$$\Omega(z) = \int_C \frac{-i\gamma(\zeta)}{2\pi(i2y_g + \zeta^* - z)}|d\zeta| \tag{14}$$

In the discretized form

$$\Omega(z) = \sum_j \tilde{w}_j(z) \tag{15}$$

where the contribution of the jth segment image is obtained from Eq. (10), replacing ζ with $i2y_g + \zeta^*$ and γ with $-\gamma$:

$$\tilde{w}_j(z) = -\frac{i\gamma_j}{2\pi}\frac{\zeta_j - \zeta_{j-1}}{|\zeta_j - \zeta_{j-1}|}\ln\frac{i2y_g + \zeta_j^* - z}{i2y_g + \zeta_{j-1}^* - z} \tag{16}$$

This value applies even when $z = \frac{1}{2}(\zeta_j + \zeta_{j-1})$ because $\tilde{w}_j(z)$ is analytic in the half-plane $\mathrm{Im}(z) > y_g$.

A horizontal shear layer, which in the limit of zero thickness becomes a surface of discontinuity, has to be treated as an additional vortex sheet inside the flowfield. If, as indicated in Fig. 2, the segment endpoints are numbered on the trailing sheet from 0 to m and on the shear layer from $m+1$ to n, the combined complex velocity is

$$w(z) = \sum_{j=1}^{m} w_j(z) + \sum_{j=m+2}^{n} w_j(z) + \psi(z) \tag{17}$$

The isolated term $\psi(z)$ in Eq. (17) is the end effect of the semi-infinite vortex sheet segments on the left of ζ_{m+1} and the right of ζ_n. To keep $\psi(z)$ finite, both semi-infinite segments must have the same density, denoted here γ_∞. Using Eq. (10) and applying the appropriate limits, the following result is obtained:

$$\psi(z) = \frac{i\gamma_\infty}{2\pi}\left[\ln\frac{\zeta_{m+1} - z}{\zeta_n - z} + i\pi\alpha(y - y_s)\right] \tag{18}$$

where y_s is the vertical location of the shear layer and α is a step function defined as

$$\alpha(p) = \begin{cases} 1, & p > 0 \\ 0, & p = 0 \\ -1, & p < 0 \end{cases} \tag{19}$$

Initially, $\mathrm{Im}\,\zeta_j = y_s$, $j = m+1, \ldots, n$, and $\gamma_j = \gamma_\infty$, $j = m+2, \ldots, n$, so that the complex velocity induced by the shear-layer segments in Eq. (17) is

$$\sum_{j=m+2}^{n} w_j(z) + \psi(z) = -\frac{1}{2}\gamma_\infty\alpha(y - y_s)$$

In the subsequent evolution of the shear layer, it is assumed that the endpoints ζ_{m+1}, ζ_n are fixed and $\psi(z)$, Eq. (18), is invariant.

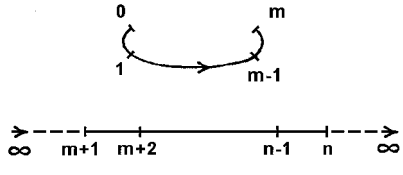

Fig. 2 Numbering of segment endpoints.

This numerical scheme is easily extended to multiple shear layers, providing a stepwise description of arbitrary crosswind profiles.

III. Time Stepping

The evolution of the discretized vortex sheet is investigated in the Lagrangian way, by tracking the displacements of segment endpoints in pseudotime τ. To bypass the logarithmic singularity, the complex velocities at segment endpoints ζ_j are evaluated as the averages of those at the surrounding midpoints:

$$w(\zeta_j) = \tfrac{1}{2}\left\{w\left[\tfrac{1}{2}(\zeta_{j-1} + \zeta_j)\right] + w\left[\tfrac{1}{2}(\zeta_j + \zeta_{j+1})\right]\right\} \tag{20}$$

Denoting by superscript k the time step, the following forward-marching scheme is obtained:

$$\zeta_j^k = \zeta_j^{k-1} + w^*\left(\zeta_j^{k-1}\right)\Delta\tau \tag{21}$$

where $\Delta\tau$ is the pseudotime increment and w^* is the complex velocity conjugate. By conservation of vorticity,

$$\gamma_j^k = \gamma_j^{k-1}\frac{\left|\zeta_j^{k-1} - \zeta_{j-1}^{k-1}\right|}{\left|\zeta_j^k - \zeta_{j-1}^k\right|} \tag{22}$$

Accordingly, when the segment stretches, its density decreases, and when it contracts, its density increases.

The described scheme is in general time irreversible, that is, a backward step does not restore the preceding position:

$$\zeta_j^k - w^*\left(\zeta_j^k\right)\Delta\tau \neq \zeta_j^{k-1}$$

An alternative "predictor-corrector" scheme has been implemented that uses a portion of the difference

$$\Delta\zeta_j^k = \zeta_j^{k-1} - \zeta_j^k + w^*\left(\zeta_j^k\right)\Delta\tau \tag{23}$$

to correct the forward step. Using this approach, the (single-step) irreversibility can be reduced and tighter-wound vortex spirals produced as a result. Also, the conservation of the first or second moments of vorticity can be controlled in this way.

The relationship between the pseudotime and the actual time is dependent upon the definition of the vortex density γ in Eq. (1a). In this paper the circulation about the wing of span b is represented by the trigonometric expansion[19]

$$\Gamma(x) = 2bU\sum_{n=1}^{\infty} A_n \sin n\theta \tag{24}$$

where the angle $\pi \geq \theta \geq 0$ is related to the spanwise coordinate x according to

$$\theta = \arccos(2x/b), \qquad -b/2 \leq x \leq b/2 \tag{25}$$

From the lifting line theory

$$A_1 = C_L/\pi AR \tag{26}$$

The physical vortex density,[20] being equal to $-\mathrm{d}\Gamma/\mathrm{d}x$, can be nondimensionalized as

$$\gamma(x) = -\frac{\pi AR}{UC_L}\frac{\mathrm{d}\Gamma(x)}{\mathrm{d}x} = 4\sum_{n=1}^{\infty} n a_n \frac{\cos n\theta}{\sin\theta} \tag{27}$$

where

$$a_n = (\pi AR/C_L)A_n \tag{28}$$

From Eq. (26) it follows that $a_1 = 1$ if $C_L \neq 0$. Further, for a symmetrical distribution of γ all even-numbered coefficients in Eq. (27) are zero.

In this way the equivalence of the roll up for wings having the same spanwise loading at different lift coefficients and aspect ratios can be exploited. However, because then the velocity described by Eq. (1a) is also nondimensional, the pseudotime τ must furnish the length dimension. From Eq. (27) the real time is obtained as

$$t = (\pi AR/UC_L)\tau \tag{29}$$

and the downstream distance

$$d = Ut = (\pi AR/C_L)\tau \tag{30}$$

Thus, if d is measured in wing-span units, then so is τ. A similar dependence of the downstream distance on AR/C_L has earlier been established by others.[21,22]

IV. Simulation Examples

The numerical examples given here were produced by a code called vortex sheet roll up, written as an interactive-graphic, object-oriented Windows application. This code creates live simulations of vortices and their interactions with ambient shear on a monitor of a personal computer. The original version[23] was implemented with Borland C++. The more recent version, which includes multiple shear layers, has been developed with Visual C++.

A straight-line vortex sheet, whose density γ is represented by the series of Eq. (27), is used as the initial condition for the calculation of vortex spirals. As expected from the natural trend towards the disappearance of tangential discontinuities, most of the segments stretch, and their density γ decreases. A counterexample is a localized contraction occurring during the formation of the inboard vortex. However, even during this short-lived event, the total length of the vortex sheet still increases.

An illustrative example in Fig. 3 shows a half of the rolling-up vortex sheet together with its vorticity histogram: vortex density γ (in a convenient scale) is plotted against the arc length coordinate of the vortex sheet. The initial value of γ, corresponding to a straight vortex sheet, was calculated from Eq. (27) using $a_1 = 1$, $a_3 = 0$, $a_5 = \sqrt{2}/10$, and $a_j = 0$ $(j > 5)$. This case, analyzed earlier by Clements and Maull,[21] is known to produce an inboard vortex near the local maximum of the vortex density.[24,25] From Fig. 3 it may be observed that the formation of the inboard vortex is preceded by a sudden peaking of γ. The peak dissolves as soon as stretching, accompanied by the inboard roll up, sets in. The spontaneous appearance of the kink (discontinuity of curvature) in the shape of the evolving vortex sheet is consistent with the theory of Moore.[26]

In Fig. 3 the dark dot and a gray verical line segment attached to it are used to indicate the center of vorticity and the path traveled. Because of a high (singular) upward velocity at the end of a straight vortex sheet, the wing-tip portion of the vortex initially moves upward. Later, the fully developed vortex catches up with its center of vorticity and moves downward with it. This may be observed in the figures to follow.

Figure 4 illustrates the numerical instability of a shear layer, above which the flow is to the right (positive direction) and below to the left (negative direction). The vortex density, determined by the jump of tangential velocity across the sheet according to Eq. (5), is in this case negative because $v_t^+ > 0 > v_t^-$. The accumulation of numerical errors goes unnoticed until a "critical" time, at which wiggles in the vortex sheet appear, followed by a rapid disintegration into a row of vortices. The discontinuities in the sheet appear only because highly stretched segments, whose $|\gamma|$ drops below a prescribed value, are not plotted. These segments may reappear if they contract and their $|\gamma|$ increases.

Because small periodic disturbances of a uniform vortex sheet are known to grow at a rate inversely proportional to their wavelength (Kelvin–Helmholtz instability), a vortex sheet with a more refined segmenting is prone to disintegrate sooner. This instability may pose problems in simulating the interactions with trailing vortices because a distant shear layer may disintegrate well before the vortices arrive. However, it is possible to keep the shear-layer segmenting coarse until the aircraft vortices arrive and then refine it for a better resolution of the induced shear layer vortices.

The evolution of a vortex spiral is quite a different matter because the stretching of the sheet, as it winds into a spiral, has a stabilizing effect.[10–12] The stability of this convection problem can be characterized by the displacement of the segment relative to its size,

$$\mathcal{C} = |w|\frac{\Delta\tau}{\Delta s} \tag{31}$$

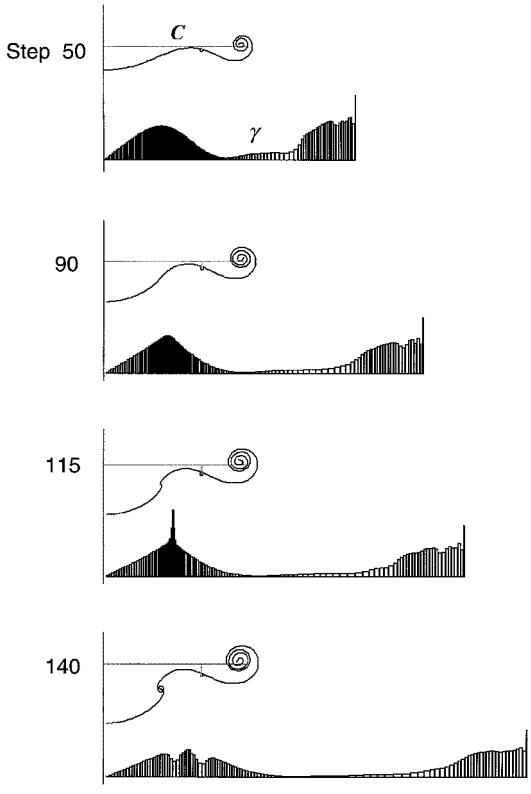

Fig. 3 Formation of an inboard vortex.

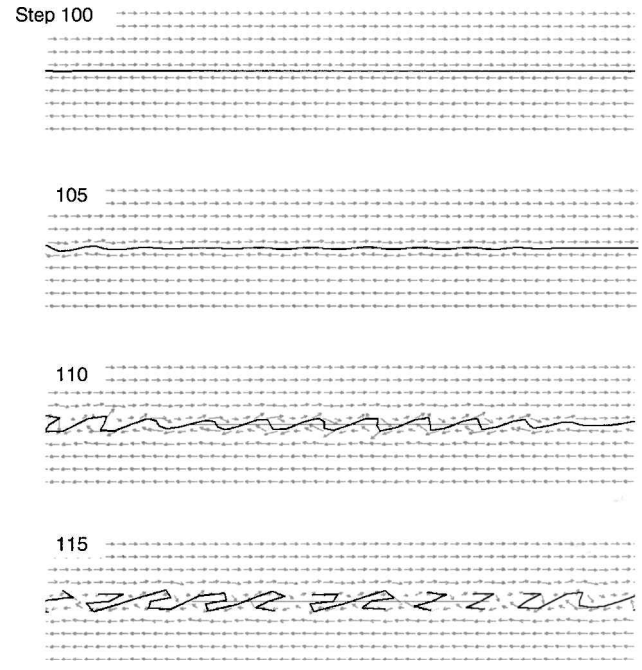

Fig. 4 Numerical instability of shear layer.

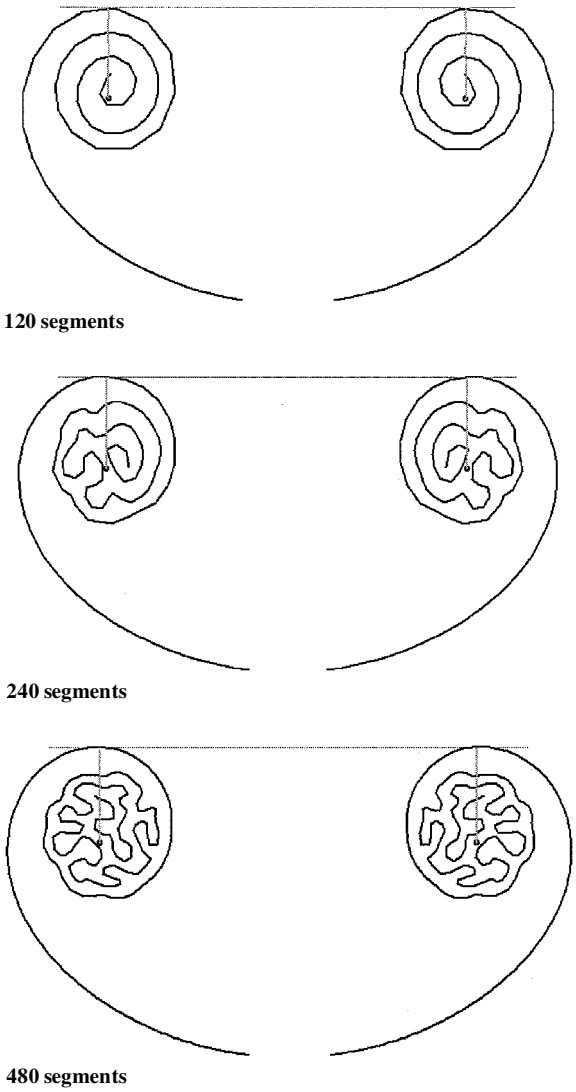

Fig. 5 Numerical instability of a vortex spiral.

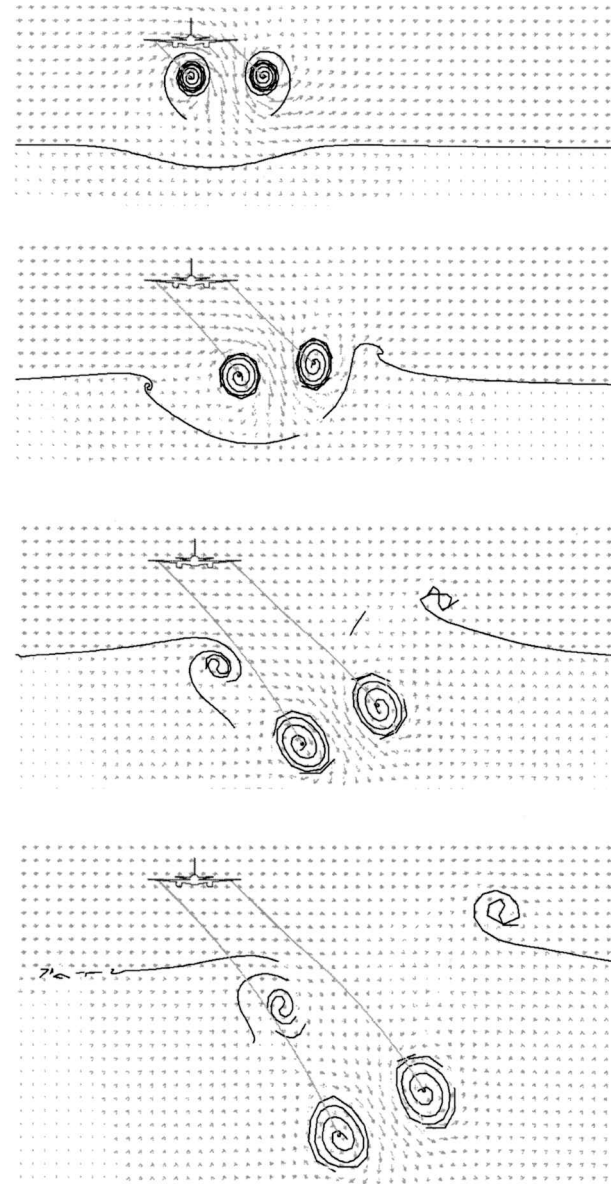

Fig. 6 Weak interaction of trailing vortices and atmospheric shear.

When using a constant time stepping, an initially unstable behavior may be observed. Eventually, the spiral stabilizes because Δs increases as a result of stretching.

The three illustrative examples in Fig. 5 were obtained for an elliptic loading, $a_1 = 1$, $a_j = 0$, $j > 1$, and cosine distribution of segments (more dense toward the wing tips). The pictures display the spirals obtained after 100 steps using a constant $\Delta\tau = 0.005$. The spiral built of 120 segments appears to be most stable. The other two spirals using a more refined segmenting are seen to develop a chaos-like labyrinth pattern filling the vortex core area. The folds of the stretched vortex sheet are similar in appearance to the curve of Peano,[27] described by a continuous function which in the limit of infinite refinement fills a rectangular domain and is nowhere differentiable.[28] From the practical point of view, the segmenting of the wing-tip portion of the vortex sheet is irrelevant because a more refined segmenting leads to a creation of a core in which the winds of the spiral, like in real physics, can no longer be identified.

The interaction of aircraft trailing vortices with shear layers, which is the main topic of this paper, is a phenomenon that has been investigated relatively recently. Based on Memphis field measurements[29] and viscous flow numerical modeling,[30] Proctor[31] observed that the interaction depends on the strength of the shear layer with respect to the strength and orientation of the aircraft vortex. The vortex may pass through the shear layer, stall, or deflect upward. Zheng and Baek,[32] assuming that the interaction is essentially of inviscid nature, duplicated these results by the method of discrete vortices.

An example of a "weak" interaction of aircraft trailing vortices with a thin atmospheric shear layer, simulated by the continuous sheet method, is shown in Fig. 6. A superposition with uniform crosswind was used to obtain zero velocity below the shear layer. The computation is started at time $\tau = 0$ by inserting a flat trailing vortex sheet of the flying-by aircraft and letting the evolution take place. The picture sequence shows that the descending aircraft vortices indent the shear layer, tear it (the highly stretched segments are not plotted), and finally pass through it. The ends of the indentation basin are seen to roll up and interact with the aircraft trailing vortices. The tilt of the aircraft vortices on passing through the shear layer makes them follow oblique paths well into the still air below.

A "strong" interaction, in which the aircraft vortices separate and couple with their shear-layer counterparts, is shown in Fig. 7. In this case the shear layer is twice as strong as in the preceding case, but no crosswind is applied. In the third and fourth frames of Fig. 7, we see that on the right-hand side the (positive) aircraft vortex and the (negative) shear layer vortex already move upward. On the left-hand side, the (negative) aircraft vortex and the (negative) shear-layer vortex enter into a slow orbiting motion about each other.

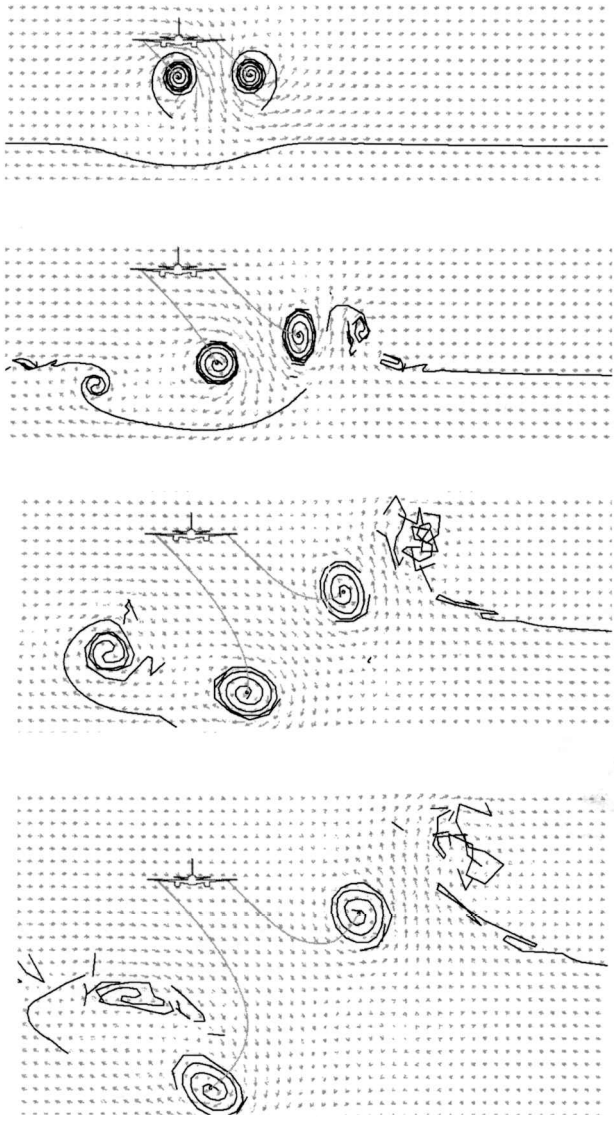

Fig. 7 Strong interaction of trailing vortices and atmospheric shear.

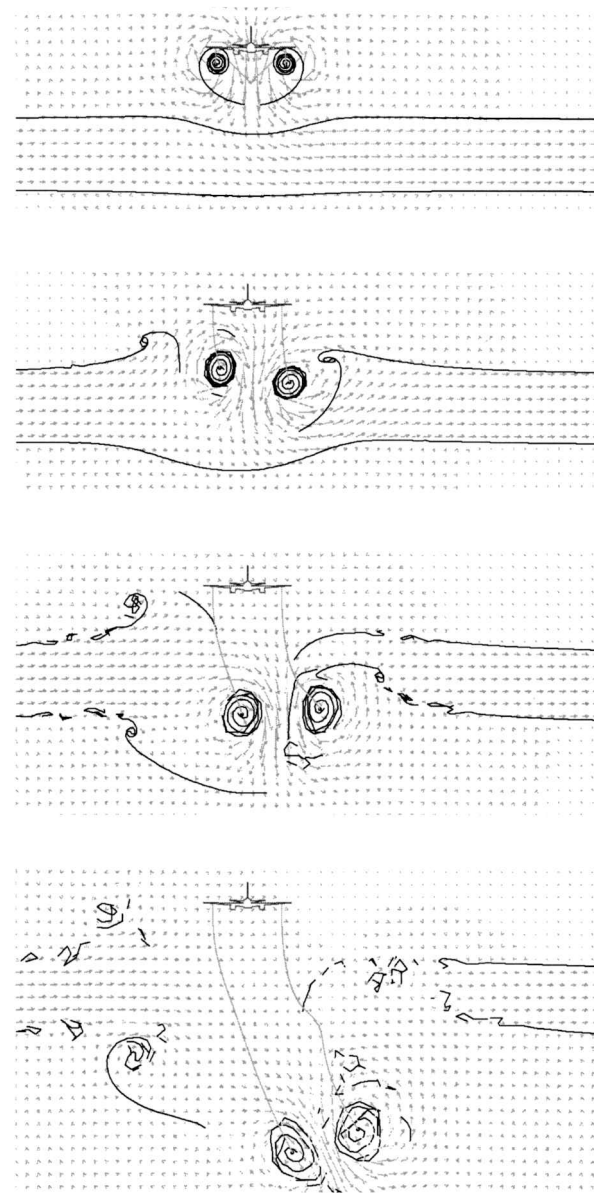

Fig. 8 Interaction of trailing vortices with air current (two horizontal, opposite-strength shear layers).

Figure 8 shows an interaction of aircraft vortices with a finite-width stream, modeled by two horizontal shear layers of opposite strength. The upper shear layer is positive, moving the air above to the left and below to the right. The lower shear layer is negative, moving the air above to the right and below to the left. The net effect of these two shear layers is still air above and below, and uniform air current to the right in between the layers.

The first frame of Fig. 8 shows the initial indentation of the shear layers as a result of the approaching aircraft vortices. In the second frame the upper shear layer is already torn, and the vortex pair is tilted in the clockwise direction. In the third frame the created upwind shear-layer vortices are seen moving apart, keeping a distance from the (negative) aircraft vortex. The downwind shear layers are seen to wrap around the (positive) aircraft vortex, making its path irregular. In the fourth frame the aircraft vortices have already crossed the stream. The vortex pair is tilted now in the anticlockwise direction and continues its descent along an oblique path into the still air below. A noninteractive superposition of the stream velocity and the self-induced motion of the aircraft vortex pair would not be able to model such effects.

A similar scheme is also applicable to investigating the interaction of the trailing vortices and a shear layer in the vicinity of ground. The horizontal symmetry is modeled by the ground images of both the aircraft trailing sheet and the shear layer. As in the preceding case, the actual shear layer and the image shear layer have opposite vortex densities; compare Eqs. (1a) and (14). The main difference is that a uniform crosswind has to be superimposed, such that the velocity between the shear layer and ground is zero. Prior to the insertion of the aircraft trailing sheet, the nonslip boundary condition at the ground is thus satisfied. The distance between the shear layer and ground should in principle correspond to the displacement thickness of the sheared flow between the aircraft and ground. In the context of discrete vortices, a similar approach has earlier been proposed by Burnham.[33]

The strengths of vortices and shear layer in the example of Fig. 9 are the same as those in Fig. 6, but the difference in the two flow patterns is readily apparent. A portion of the shear layer scooped by the downwind vortex rolls up into a vortex of opposite orientation. The mutual interaction makes the aircraft vortex rise and the weaker shear-layer vortex orbit about the former.[34] The path of the trailing vortex is wavy but nonperiodic because the scooping of the shear layer is a continuing process. In this case the upwind vortex is practically stalled over the runway, acting as a barrier to the advancing shear layer. We may note that the resultant contraction of the upwind portion of the shear layer has a destabilizing effect, forcing it to disintegrate into a row of ground-level vortices.

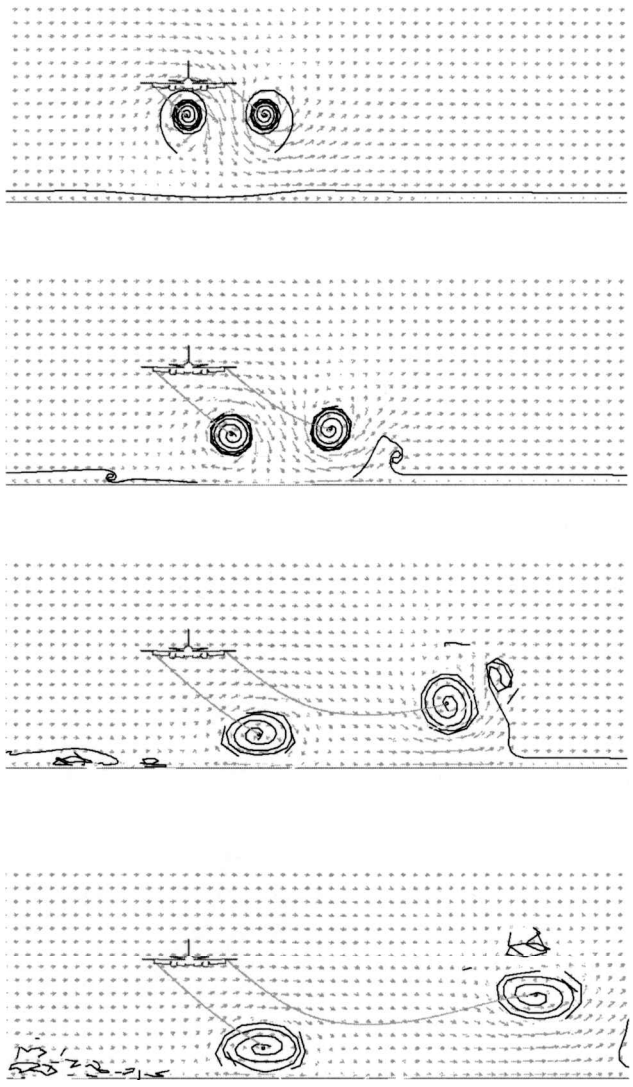

Fig. 9 Interaction of trailing vortices and ground shear.

As pointed out in the Introduction, the current version of the method conserves vorticity and can only be applied to the existing ground shear as a result of crosswind and not to that induced by the approaching aircraft vortices. Nevertheless, the obtained results are very encouraging, predicting vortex bounce[35] and other observable phenomena without resorting to the empiricism of the vortex forecasting methods in which the ground vortices are "implanted."

Concerning the real-time simulation of aircraft vortices, there is clearly a limit on the number of representing segments that can be used with a given compiler or processor. Because each segment contributes to the motion of other segments in a linear fashion, the number of numerical operation is proportional to the number of segments squared. However, when a larger number of segments are used, a smaller $\Delta\tau$ may also be necessary in order to suppress the initial irregularities in vortex spirals. Based on the 1-GHz processor as a standard, no example in this paper required more than 5 min of computer time.

V. Conclusions

It has been demonstrated that a number of phenomena related to the evolution and convection of aircraft trailing vortices can be modeled in a simplified form by the surfaces of discontinuity in potential flow. Among those are the encounters of trailing vortices with atmospheric and ground shear layers. It is believed that this computationally efficient method offers an alternative to the currently used semi-empirical algorithms for real-time forecasting of aircraft trailing vortices. A copy of the software, used to produce the examples in this paper, is available from the author upon request.

Acknowledgments

This project has been carried out under the Vortex Dynamics Program of the Institute for Aerospace Research. The author gratefully acknowledges Bill Rainbird for helpful discussions during the writing of the original version[23] and the anonymous referees for their substantive comments and suggestions, including the present title of the paper.

References

[1]Mokry, M., and Rainbird, W. J., "Calculation of Vortex Sheet Roll-up in a Rectangular Wind Tunnel," *Journal of Aircraft*, Vol. 12, No. 5, 1975, pp. 750–752.

[2]Rosenhead, L., "The Formation of Vortices from a Surface of Discontinuity," *Physics of Fluids A*, Vol. 5, No. 11, 1933, pp. 170–192.

[3]Westwater, F. L., "The Rolling up of the Surface of Discontinuity Behind an Aerofoil of Finite Span," Aeronautical Research Council R&M 1692, U.K., Aug. 1935.

[4]Prandtl, L., and Tietjens, O. G., *Fundamentals of Hydro- and Aeromechanics*, Dover, New York, 1957, p. 216.

[5]Baker, G. R., and Shelley, M. J., "On the Connection Between Thin Vortex Layers and Vortex Sheets," *Journal of Fluid Mechanics*, Vol. 215, 1990, pp. 161–194.

[6]Lamb, H., *Hydrodynamics*, 6th ed., Cambridge Univ. Press, 1932, pp. 373–375.

[7]Meiron, D. I., Baker, G. R., and Orszag, S. A., "Analytic Structure of Vortex Sheet Dynamics; Part 1. Kelvin-Helmholtz Instability," *Journal of Fluid Mechanics*, Vol. 114, 1982, pp. 283–298.

[8]Caflisch, R. E., and Orellana, O. F., "Long Time Existence for a Slightly Perturbed Vortex Sheet," *Communications on Pure and Applied Mathematics*, Vol. 39, 1986, pp. 807–838.

[9]Birkhoff, G., "Helmholtz and Taylor Instability," *Physics of Fluids A*, Vol. 5, Nov. 1993, pp. 55–76.

[10]Moore, D. W., and Griffith-Jones, R., "The Stability of an Expanding Circular Vortex Sheet," *Mathematika*, Vol. 21, 1974, pp. 128–133.

[11]Moore, D. W., "The Stability of an Evolving Two-Dimensional Vortex Sheet," *Mathematika*, Vol. 23, 1976, pp. 35–44.

[12]Saffman, P. G., *Vortex Dynamics*, Cambridge Univ. Press, 1992, pp. 142–145.

[13]Sarpkaya, T., "Decay of Wake Vortices of Large Aircraft," *AIAA Journal*, Vol. 36, No. 9, 1998, pp. 1671–1679.

[14]Mokry, M., "Real-Time Simulation of Aircraft Wake Vortices," *Proceedings of the 5th Annual Conference of the CFD Society of Canada*, 1997, pp. 9.15–9.20.

[15]Darracq, D., Moet, H., and Corjon, A., "Effect of Crosswind Shear and Atmospheric Stratification on Aircraft Trailing Vortices," AIAA Paper 99-0985, Jan. 1999.

[16]Muskhelishvili, N. I., *Singular Integral Equations*, Noordhoff-Groningen, Leyden, The Netherlands, 1953, pp. 42, 43.

[17]Gakhov, F. D., *Boundary Value Problems*, Pergamon, New York, 1966, pp. 13–16.

[18]Berker, R., "Intégration des Équations du Mouvement d'un Fluide Visqueux Incompressible," *Encyclopedia of Physics*, edited by S. Flügge, Springer-Verlag, 1963, pp. 112–125.

[19]Katz, J., and Plotkin, A., *Low-Speed Aerodynamics*, McGraw-Hill, New York, 1991, pp. 207–210.

[20]Lam, F., "Induced Drag of Wings of Finite Aspect Ratio," *AIAA Journal*, Vol. 31, No. 2, 1993, pp. 396–398.

[21]Clements, R. R., and Maull, D. J., "The Rolling Up of a Trailing Vortex Sheet," *Aeronautical Journal*, Vol. 77, Jan. 1973, pp. 46–51.

[22]Jumper, E. J., and Nelson, R. C., "Computing the Near-Field Dynamics of the Wake," *Proceedings of the International Wake Vortex Meeting*, Transportation Development Centre, TP-13166, Ottawa, Ontario, Dec. 1997, pp. 95–104.

[23]Mokry, M., "Numerical Simulation of Aircraft Trailing Vortices in an Interactive Graphics Environment," AIAA Paper 99-0827, Jan. 1999.

[24]Donaldson, C. duP., Snedeker, R. S., and Sullivan, R. D., "Calculation of Aircraft Wake Vorticity Profiles and Comparison with Experimental Measurements," *Journal of Aircraft*, Vol. 11, No. 5, 1974, pp. 547–555.

[25]Hoeijmakers, H. W. M., "Vortex Wakes in Aerodynamics," AGARD CP-584, May 1996, pp. 1.1–1.12.

[26]Moore, D. W., "The Spontaneous Appearance of a Singularity in the Shape of an Evolving Vortex Sheet," *Proceedings of the Royal Society*

London A, Vol. 365, 1979, pp. 105–119.

[27]Peano, G., "Sur une Curbe, qui Remplit Toute une Aire Plane," *Math. Annalen*, Vol. 36, 1890, pp. 157–160.

[28]Hairer, E., and Wanner, G., *Analysis by Its History*, 2nd ed., Springer-Verlag, 1997, pp. 263–270, 290–298.

[29]Campbell, S. D., Dasey, T. J., Freehart, R. E., Heinrichs, R. M., Matthews, M. P., and Perras, G. H., "Wake Vortex Field Measurement Program at Memphis, TN," AIAA Paper 96-0399, Jan. 1996.

[30]Proctor, F. H., Hinton, D. A., Han, J., Schowalter, D. G., and Lin, Y. L., "Two Dimensional Wake Vortex Simulation in the Atmosphere: Preliminary Sensitivity Studies," AIAA Paper 98-0056, Jan. 1997.

[31]Proctor, F. H., "The NASA-Langley Wake Vortex Modelling Effort in Support of an Operational Aircraft Spacing," AIAA Paper 98-0589, Jan. 1998.

[32]Zheng, Z. C., and Baek, K., "Inviscid Interactions Between Wake Vortices and Shear Layers," *Journal of Aircraft*, Vol. 36, No. 2, 1999, pp. 477–480.

[33]Burnham, D. C., "Effect of Ground Wind Shear on Aircraft Trailing Vortices," *AIAA Journal*, Vol. 10, No. 8, 1972, pp. 1114, 1115.

[34]Spalart, P. R., "Airplane Trailing Vortices," *Annual Reviews of Fluid Mech.*, Vol. 30, 1998, pp. 107–138.

[35]Harvey, J. K., and Perry, F. J., "Flowfield Produced by Trailing Vortices in the Vicinity of the Ground," *AIAA Journal*, Vol. 9, No. 8, 1971, pp. 1659–1661.